2021

Accuracy of novel image acquisition and processing device in automatic segmentation of atopic dermatitis

BOSTON UNIVERSITY

SCHOOL OF MEDICINE

Thesis

ACCURACY OF NOVEL IMAGE ACQUISITION AND PROCESSING DEVICE

IN AUTOMATIC SEGMENTATION OF ATOPIC DERMATITIS

by

MATT LONDON

B.A., San Jose State University, 2015

Submitted in partial fulfillment of the

requirements for the degree of

Master of Science

2021

Approved by

First Reader   _____

Kevin Thomas, Ph.D.
Director, Healthcare Emergency Management Program Director,
Masters of Science in Bioimaging Assistant Professor, Anatomy and
Neurobiology

Second Reader   _____

Nina Kabiri, Ph.D.
Research Scientist, Anatomy and Neurobiology

ACCURACY OF NOVEL IMAGE ACQUISITION AND PROCESSING DEVICE IN AUTOMATIC SEGMENTATION OF ATOPIC DERMATITIS

MATT LONDON

ABSTRACT

Atopic Dermatitis (AD), a chronic inflammatory skin disease causing lesions, often causes decreased quality of life (Kapur, 2018). Segmentation, a method of illustrating the difference between lesioned and non-lesioned areas of interest (AOIs) has been the primary method for which AD has been studied (Ranteke & Jain, 2013). Manual segmentation is prone to subjectivity (Ning et al., 2014) and automatic segmentation, while reliable and efficient, poses challenges such as light reflections and color variations (Lu et al., 2013). Yet, AD can be classified from color and texture (Hanifin et al., 2001; Nisar et al., 2013), as well as through machine learning methods. The purpose of this study was to determine the optimal method for segmentation of images of atopic dermatitis on subject arms in a novel and standardized photography lightbox (Lightbox) and of images of subjects' self-acquired at-home photos. The goals of this study were to determine the accuracy and reliability of photo acquisition of arms of subjects with AD in a novel standardized photography lightbox, compared to photo acquisition by subjects at home, and determine the accuracy and reliability of automated segmentation of AD lesions with combined color-based segmentation and the U-Net CNN.

TABLE OF CONTENTS

LIST OF FIGURES

LIST OF ABBREVIATIONS

AD   Atopic Dermatitis

AOI   area of interest

CIELAB   Commission Internationale de l'Eclairage:

                                                       luminosity, green-red, blue-yellow

CMY   cyan, magenta, yellow

CNN   convolutional neural network

CPU   central processing unit

EASI   Eczema Area and Severity Index

FIJI   FIJI Is Just ImageJ

GPU   graphics processing unit

HRPP   Human Research Protection Program

HSI   hue, saturation, intensity

NPV   negative predictive value

PPV   positive predictive value

RGB   red, green, blue

ROI   region of interest

SCORAD   Scoring Atopic Dermatitis Index

YCbCr   luma, blue-difference, red-difference

INTRODUCTION

Atopic Dermatitis (AD), a chronic inflammatory skin disease causing lesions, often causes decreased quality of life (Kapur, 2018). Currently, there is no known cure for atopic dermatitis. Consequently, there is much research and development of treatments for the symptoms of AD (Weidinger & Novak, 2016). Determining AD severity and rate of pathology is essential to developing treatments and managing care (Oranje et al., 2007). Segmentation of AD lesions is the primary method that AD severity has been determined (Nisar et al., 2013). Quantification of AD severity comprises segmenting lesioned from non-lesioned regions in AOIs and measuring the pathological rate of change of the AD lesion. Up to the early 1990s, segmentation had been undertaken manually by practitioners and demonstrated low reliability, due to its highly subjective process (Ben-Gashir et al., 2004). In the early 1990s, standardized AD severity scales were introduced (Kunz et al, 1997). Popular scales include the Scoring Atopic Dermatitis Index (SCORAD) and the Eczema Area and Severity Index (EASI) (Nisar et al., 2013). The EASI classifies AD lesions into four primary factors: erythema (redness), edema (swelling), excoriation (scratch damage), and/or lichenification (thick, leathery skin) (Alam et al., 2016). Furthermore, each factor is categorized on a scale of 0-4 (none, mild, moderate, severe). The EASI and SCORAD have exhibited good inter- and intra-rater reliability in some studies (Barbier et al., 2004; Hanifin et al., 2001). Yet, other studies concluded that, due to the subjective bias of severity scales, they cannot be considered to be reliable across different studies (Ben-Gashir et al., 2004; Ning et al., 2014).

1

Within the past decade, automated segmentation algorithms have been developed to improve the reliability and efficiency of segmentation for atopic dermatitis lesions (Nisar et al., 2013; Ch'ng et al., 2014). Popular segmentation algorithms comprise thresholding, clustering, growing, region merging, and edge detection. Furthermore, transformation of RGB images to other color spaces, prior to color and texture segmentation, can give superior segmentation results (Ch'ng et al., 2014; Hanifin et al., 2001; Nisar et al., 2013).

K-means clustering is a favored clustering method, due to speed and accuracy (Nisar et al., 2013; Ch'ng et al., 2014). K-means clustering identifies diverse spectral groups contained in a data set, using a select number of k clusters and randomly selected k-cluster centers (Figure 1). The Euclidean function determines the range between each pixel and all cluster centers. Each pixel is allocated to the closest cluster center. The cluster center is randomly chosen and the Euclidean function run to allocate pixels until there is no more change in pixel allocation.

$$J = \sum_{j=1}^{k} \sum_{i=1}^{n} \left\| x_i^{(j)} - c_j \right\|^2$$

Figure 1. Equation for K-means clustering

Nisar et al. (2013), in their research for the optimal automated system for AD segmentation, transformed RGB (Red, Green, Blue) photographs of AD infested skin to grayscale, segmented skin from the background with Otsu thresholding, transformed segmented skin region from RGB to four select color spaces, and segmented AD from healthy skin with k-means clustering. The four color spaces comprised HSI (hue, saturation, intensity), CMY (Cyan, Magenta, Yellow), YCbCr (Y is luma component, Cb and Cr are the blue-difference and red-difference chroma components), and CIELAB (a.k.a. L*a*b*; CIE signifies Commission Internationale de l'Eclairage, an organization that establishes standard color values to be used on an international level; L* describes luminance; a* describes degree of green to red; and b* represents degree of blue to yellow) (*Figure 2*).

The HSI color space model (aka HSV (Hue, Saturation, Value) is most akin to how the human eye discerns color. "H" (Hue) is defined as the primary color/wavelength recognized by a viewer. "S" (Saturation) describes the proportion of impurity in a color.

In the L*a*b* color space model, L* is the vertical axis and represents brightness values from black to white color and ranges from 0 to 100, respectively. The horizontal axes comprise a* and b*, at 90° relative to each other. The a* axis ranges from green (-128) to red (+127). The b* axis ranges from blue (-128) to yellow (+127).
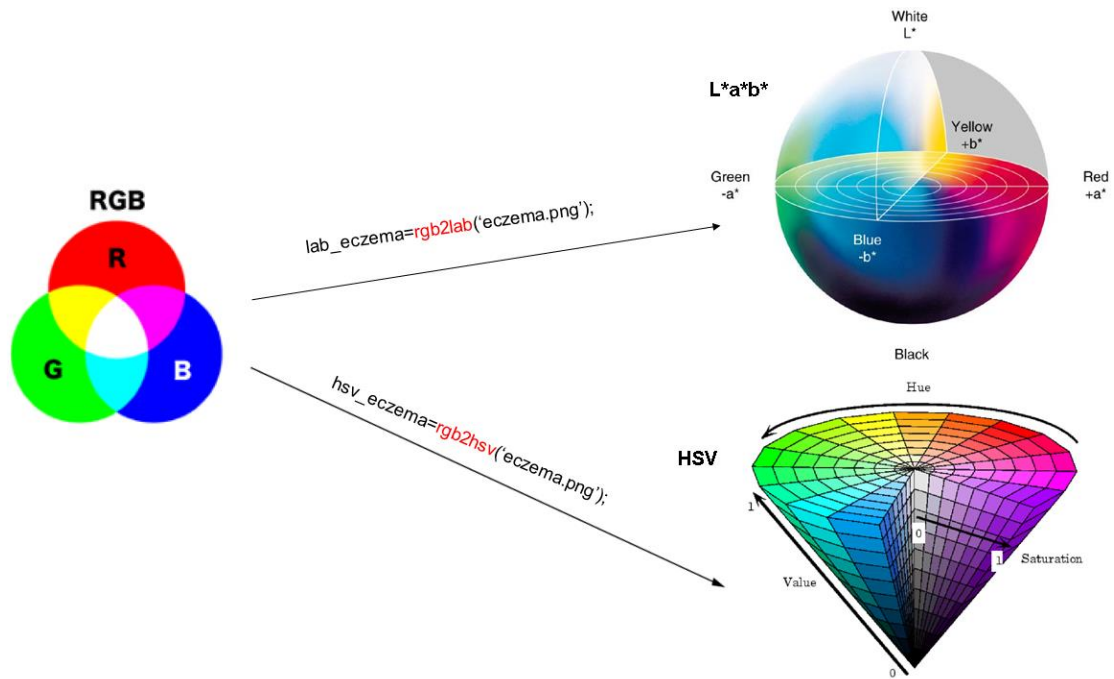
Figure 2. RGB color space transformed to L*a*b* and HSV color space with Matlab script

Nisar et al. (2013) compared transformed and segmented images against manually segmented ground truth images. Accuracy was scored with sensitivity (probability that algorithm correctly identifies AD), specificity (probability that algorithm correctly identifies healthy skin), positive predictive value (PPV; extent that subjects are correctly diagnosed with AD), negative predictive value (NPV; extent that subjects are correctly determined to not have AD), and accuracy (proportion of lesion accurately recognized). Results showed that the "H" color channel of HSI and the "a" color channel of L*a*b* afforded the most accurate k-means automated segmentation.

4

Building off Nisar et al. (2013), Ch'ng et al. (2014) utilized k-means clustering of L*a*b* images of AD. In addition, Ch'ng et al. (2014) normalized the color spaces and utilized adaptive light compensation and gamma correction to afford better segmentation. Furthermore, AD severity was determined with Z-test, which classified AD severity as either none, mild, moderate, or severe. "H" of HSI, which describes color value, is utilized for this classification. The ground truth images, produced via manual segmentation, were used to establish mean and standard deviation of intensity for each severity level. Similar to Nisar et al. (2013), images were scored with sensitivity, specificity, positive predictive value, negative predictive value, and accuracy. Results showed that adaptive light compensation afforded more accurate segmentation. Normalization afforded best accuracy for the "G" channel of RGB and "L" of L*a*b*. The green part of the a* spectrum and "G" afforded the most accurate segmentation in Nisar et al. (2013) and Ch'ng et al. (2014), respectively. This is likely due to the "G" layer of RGB containing less noise than other layers (Ch'ng et al., 2014).

Automatic segmentation, while reliable and efficient, poses challenges such as light reflections, hair, vignetting, and color variations in lesioned and non-lesioned areas of interest.

(AOIs). Furthermore, common AD AOIs (e.g. flexures, wrists, and ankles), were found to be difficult to accurately document via photograph (Weidinger & Novak, 2016).

Thus, strict standardization of photographic methods has been necessary for segmentation via k-means clustering.

Convolutional neural networks (CNNs) have gained popularity in recent years, for use in automated segmentation, due to improved software and hardware that affords efficient and precise images, regardless of confounding objects in photographs (Pal et al., 2018a, Pal et al., 2018b). U-Net, developed for biomedical image segmentation, is an exceptionally fast and precise CNN (Ronneberger, 2015). Since its inception, U-Net has shown good performance in many biomedical applications, ranging from microscopic cell segmentations (Çiçek et al. 2016; Falk et al. 2019), to brain imaging (Dong et al., 2017; Salehi et al. 2017), to whole-body imaging (Andersson, 2019). Although most laptops utilizing a CPU, can segment a 512*512 in ~1 second, a GPU can segment a similar image 2x-5x faster (Aijun et al., 2004; Mehrtash et al., 2017). Most laptops and desktops do incorporate a graphics card to run a GPU. Although, these systems have yet to smoothly operate U-Net and other CNN architectures. Currently U-Net runs smoothly on CPUs and has proven successful on the CPUs of mobile devices.

The goals of this study were to determine the accuracy and reliability of photo acquisition of arms of subjects with AD in a novel standardized photography lightbox, compared to photo acquisition by subjects at home, and determine the accuracy and reliability of automated segmentation of AD lesions with combined color-based segmentation and the U-Net CNN run on a CPU.

METHODS

In accordance with the HRPP Policies of Boston University Medical Campus (BUMC), BUMC Institutional Review Board (IRB) approval was obtained prior to subject recruitment. Subjects were screened to include only those who currently used a topical treatment for atopic dermatitis (AD). Subjects who met this requirement could also be taking oral AD treatment.

Subjects ($N = 10$) were investigated for the pathological rate of AD over the course of a consecutive 22 day period. On lab visit (Visit) 1, 4, and 5, in the Laboratory of Human Neurobiology (HUB Lab), photos of the subject's arm, including AD lesions, were acquired via iPad camera (6th generation, year 2018, 9.7" screen, camera resolution: 8MP, 264ppi (10.4ppmm)) suspended in a novel photography lightbox (Lightbox; *Figure 3*). Each subject was instructed to place their right arm, fingers spread, on the floor of Lightbox, with their antecubital (inner elbow) at the 3" mark. Coronal photos of lesions were acquired as a primary point of reference. Sagittal photos of lesions were acquired to aid in lesion detection in the coronal photos. *Figure 3* shows view of light box from perspective of subject. *Figure 4* shows view of lightbox from perspective of lab technician while acquiring subject's photo. *Figure 5* shows photos from lab visit 1 of Subjects 1 and 2.

Subjects were sent home with an iPad and instructed to photograph the same arm that was photographed in Lightbox, in the coronal view, at the same time each day (Day) that they were not in the lab. 3 of 10 subjects completed at home photographs.

Photographs, acquired in lab, were compared against photographs acquired by subjects at home. Both photo sets were used to assess the feasibility of using a standardized photography method and automated segmentation to assess AD disease severity and prognosis. *Figure 6* shows at-home photos of Day 2 for Subjects 1 and 2. As part of a larger study on behavior, subjects were required to wear actigraphy devices during some of the photo acquisitions. Thus, these artifacts were accounted for in lesion segmentation.

Figure 3. Lightbox, a novel and standardized photography lightbox

Figure 4. Subject arm placement in Lightbox


Subject 1
Visit 1

Subject 2
Visit 1

Figure 5. Lightbox photos

Figure 6. At-Home photos

A dermatologist used FIJI software to manually trace AD lesions and classify the four primary factors of AD: erythema (redness), edema (swelling), excoriation (scratch damage), and/or lichenification (thick, leathery skin). The dermatologist tracings were used as ground truth ROIs when determining performance of automated segmentation. FIJI was also used to generate descriptive statistics. Mean, minimum, maximum and standard deviation of pixel values from various color spaces were used to determine thresholding values for color-based k-means clustering to mask the subject arm from the lightbox. Color-based k-means clustering of the green channel of a* and b* (of L*a*b* color space) afforded the most accurate and reliable arm masking. This provided an efficient way to obtain binay images of total arm area for photos from Lightbox. At-home photos were segmented with color-based k-means clustering, as well, yet the high amount of noise in the masks made it necessary to perform some manual correction of the at-home masks. followed by overlaying ROIs produced in FIJI, and calculating percentage

10

of arm affected by AD. *Figure 7* shows FIJI regions of interest (ROIs) overlayed

Subject's 1 and 2 Lightbox arm masks from Visit 1. *Figure 8* shows FIJI regions of

interest (ROIs) overlayed at-home arm masks of Day 2 for Subjects 1 and 2, exhibiting

arm masks before manual correction compared to after manual correction.

Subject 1
Visit 1

Subject 2
Visit 1
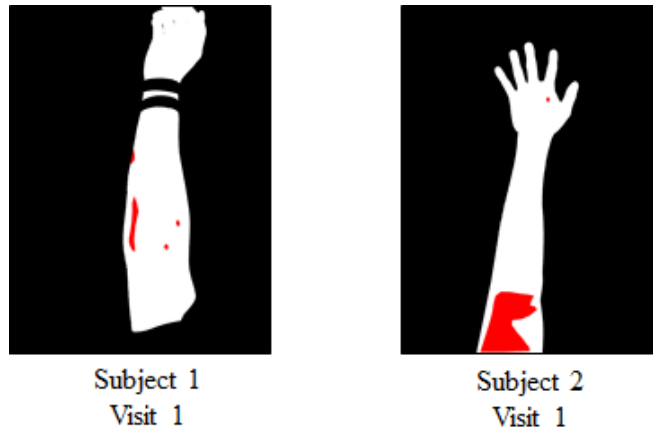
Figure 7: Lightbox arm masks overlayed with ground truth ROIs (red)
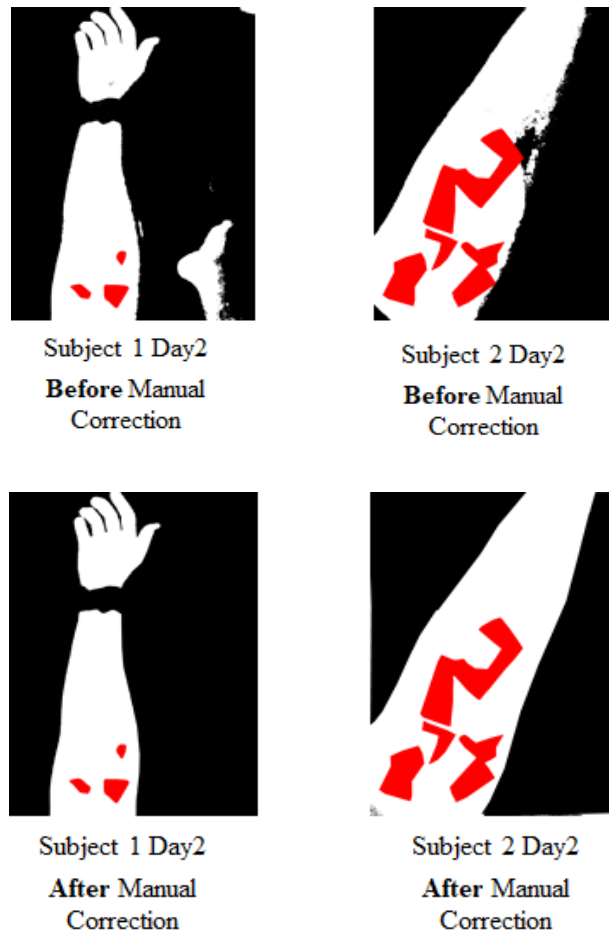
*Figure 8*: At-home arm masks overlayed with ground truth ROIs (red)

The U-Net machine learning model was deployed with Keras, with a Tensorflow

backend, with Python 3.7.4 in The Scientific Python Development Environment (Spyder)

3.3.6. All software was run on an ASUS ROG GU502GV laptop with a 9th Gen Intel®

Core™ i7-9750H CPU @ 2.60GHz, 6 cores, 12 logical processors, 16 GB RAM, 2592

MHz max clock speed, and 141pixels per inch (ppi) display resolution. The training

images for U-Net comprised photos acquired in Lightbox, converted to grayscale (pixel

values 0-255 (black-white)) ($N = 24$). Of the nine subjects, 24 photos were acquired in

Lightbox. Each subject provided 1-4 photos over the course of 1-5 days in, 1-3 day

intervals. The training ROIs (labels), which had been manually segmented by a

dermatologist, were binary images (pixel values 0 and 1 (black and white)). Test images

comprised subjects' self-acquired at-home photos, converted to grayscale ($N = 14$). Of the

three subjects who provided at-home photos, 14 photos were acquired. Each subject

provided 2-4 photos over the course of 1-5 days, in 1-3 day intervals 1 All images were

converted to 512 x 512px for efficient convolution of the U-Net neural network.

The U-Net machine learning model was deployed with Keras, with a Tensorflow

backend, with Python 3.7.4 in The Scientific Python Development Environment (Spyder)

3.3.6. All software was run on an ASUS ROG GU502GV laptop with a 9th Gen Intel®

Core™ i7-9750H CPU @ 2.60GHz, 6 cores, 12 logical processors, 16 GB RAM, 2592

MHz max clock speed, and 141pixels per inch (ppi) display resolution. The training

images for U-Net comprised photos acquired in Lightbox, converted to grayscale (pixel

values 0-255 (black-white)) ($N = 24$). Of the nine subjects, 24 photos were acquired in

Lightbox. Each subject provided 1-4 photos over the course of 1-5 days in, 1-3 day

intervals. The training ROIs (labels), which had been manually segmented by a

dermatologist, were binary images (pixel values 0 and 1 (black and white)). Test images

comprised subjects' self-acquired at-home photos, converted to grayscale ($N = 14$). Of the

three subjects who provided at-home photos, 14 photos were acquired. Each subject

provided 2-4 photos over the course of 1-5 days, in 1-3 day intervals 1 All images were

converted to 512 x 512px for efficient convolution of the U-Net neural network.

U-Net ROI predictions were rendered in grayscale (0-255 (black-white)), which were converted to binary (0, 1 (black, white)) for ROI area measurement. The binary threshold for grayscale values was 245, which converts all pixel values > 245 to 255 and all pixel values ≤ 245 to 0. was chosen as the threshold because it rendered the most accurate images with minimal noise. Pixel classification comprised black pixels in ROIs as true positive (TP) AD lesions. Black pixels outside ROIs were classified as false positive (FP). 245. *Figure 9* illustrates the process of test image augmentation, binarized thresholding of prediction, and prediction measurement.
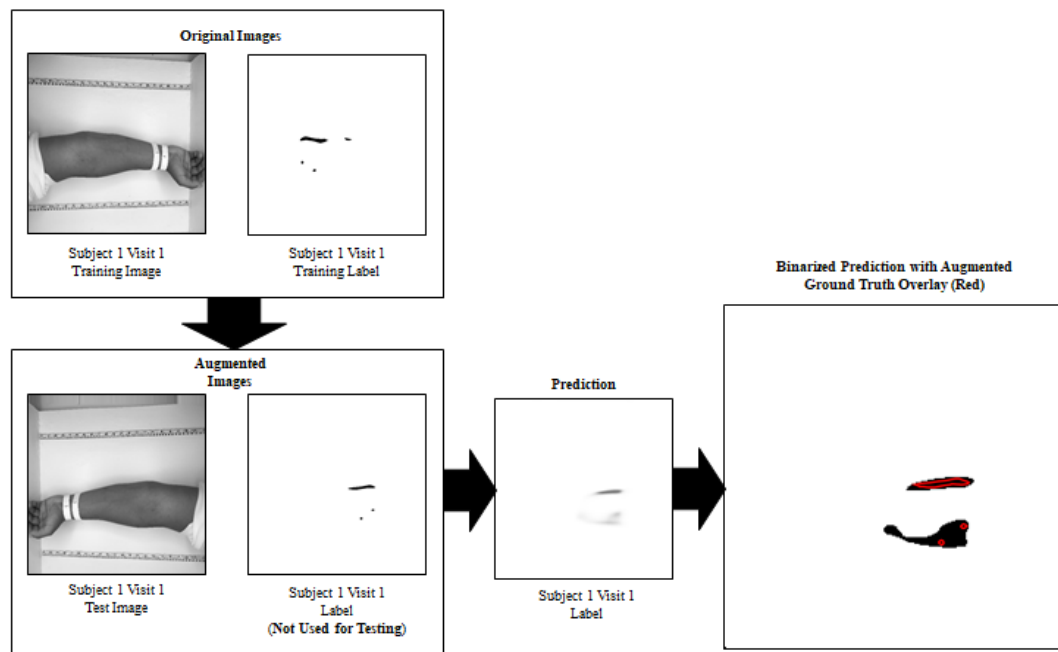
Figure 9. Subject 1 Day 1, original photo and ROIs compared to augmented photo and augmented ROIs

Positive predictive value (PPV) was used to determine the accuracy of lesion predictions, compared to ground truth ROIs (Equation 1)
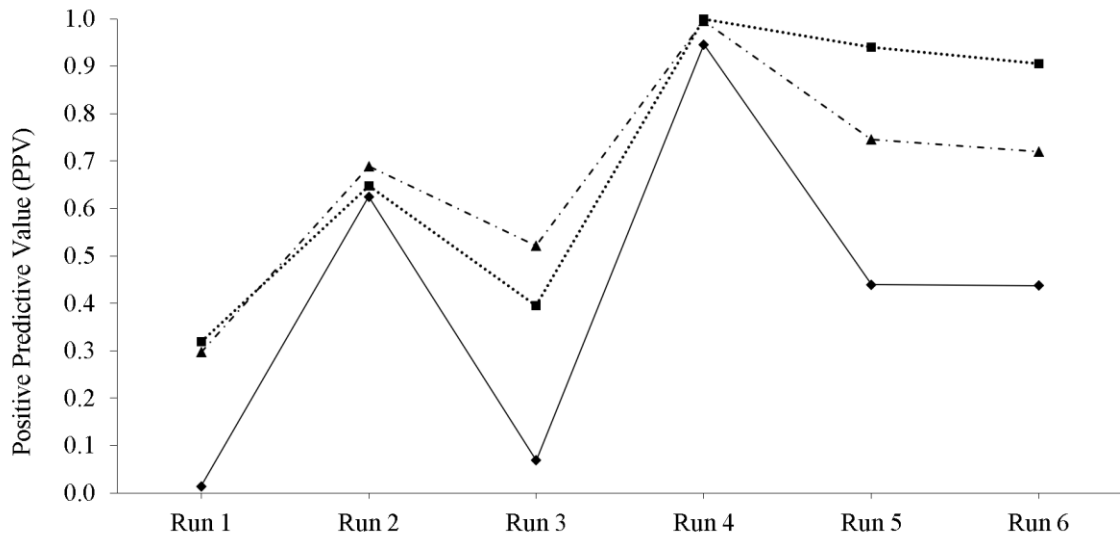
$$\text{Positive Predictive Value} = TP/(TP+FP) \qquad (1)$$

Following determination of the most accurate U-Net run, predictions from that run were measured to determine the degree of accuracy. With a threshold of 245 for binary conversion of predictions, the amount of lesion pixel, in the thresholded lesion predictions, were divided by the total amount of arm pixels, in the binary arm masks, to obtain the percentage that the lesion affected arm. Total lesion coverage percentage, as well as AD lesions of specific factor type and severity were measured to determine the accuracy, reliability, and prognosis power of automated segmentation with combined color-based segmentation and the U-Net Convolutional Neural Network.

RESULTS

Following calibration of the U-Net model for optimal speed and accuracy, 6 epochs with 40 steps-per-epoch (spe) were found to generate accurate lesion predictions with 0.9965 (±0.0015) accuracy and 0.0152 (±0.0023) loss in 4 hrs (±10 mins). Less epochs and/or spe were found to generate less accurate predictions. More epochs and/or spe were found to result in overfitting, resulting in less accurate predictions as well.

Mean PPV fluctuated across runs for images from Lightbox (*Figure 9*). High reliability of the U-Net model was evinced by negligible (<0.0001) standard deviation PPV, between predictions within each U-Net run and between U-Net runs.

Figure 10. Positive predictive values (PPVs) between subjects for U-Net AD prediction in test images

Run 4 was used to calculate and predict lesion type and severity in Lightbox photos, due to PPV being most accurate and reliable for this U-Net run.

Percentage of anatomy affected by AD lesions, across subjects, showed no significant difference between ground truth ($M = 7.48\%$, $SD = .03\%$) and Run 4 predictions ($M = 6.96\%$, $SD = .06\%$), ($t(9) = 2.46$, $p = 0.87$).

The percentage that each lesion affected, across subjects in Lightbox, showed no significant difference between ground truth ($M = 5.56\%$, $SD = .04\%$) and Run 4 predictions ($M = 4.65\%$, $SD = .06\%$), ($t(35) = 2.06$, $p = 0.63$).

Of the four primary factors of AD severity, only erythema and lichenification were expressed by the subjects. Some of the lesions contained a combination of both. Erythema was the only factor expressed exclusively, as level 1 (Ery1) and level 2 (Ery2). Lichenification severity was expressed as level 1 (Lic1) and level 2 (Lic2).

Percentage covered by Ery1, across subjects in Lightbox, showed no significant difference between ground truth ($M = 1.56\%$, $SD = .05\%$) and Run 4 predictions ($M = 1.34\%$, $SD = .04\%$), ($t(57) = 2.07$, $p = 0.65$).

Percentage covered by Ery2, across subjects in Lightbox, showed no significant difference between ground truth ($M = 1.52\%$, $SD = .01\%$) and Run 4 predictions ($M = 1.45\%$, $SD = .03\%$), ($t(14) = 2.17$, $p = 0.94$).

Percentage covered by Lic1, across subjects in Lightbox, showed no significant difference between ground truth ($M = 4.93\%$, $SD = .02\%$) and Run 4 predictions ($M = 3.73\%$, $SD = .01\%$), ($t(13) = 2.30$, $p = 0.56$).

Percentage covered by Lic2, across subjects in Lightbox, showed no significant difference between ground truth ($M = 3.09\%$, $SD = .01\%$) and Run 4 predictions ($M = 3.67\%$, $SD = .02\%$), ($t(7) = 2.71$, $p = 0.25$).

DISCUSSION

The accuracy and reliability of automated segmentation with combined color-based segmentation and the U-Net CNN was evinced by the statistical significance in the similarity of AD lesion predictions of U-Net and ground truth manually traced ROIs. These results support the finding of Lu et al. (2013) that automatic segmentation algorithms provide superior efficiency of segmentation for atopic dermatitis lesions, compared to manual segmentation, which is much more time consuming and also prone to subjective bias (Ben-Gashir et al., 2004; Ning et al., 2014).

The binary arm mask is extremely efficient for segmenting the subject's arm from the background. Thus, affording easy calculation of the number of pixels comprising the arm, which can be utilized in determining the percentage of the arm that the AD lesions affect.

The potential for a more reliable and efficient method for segmentation and quantification of pathological rate of AD, exhibited by this study, supports the work for the effective treatments for AD, described by Weidinger & Novak (2016). Although there is no known cure for AD, optimized automatic segmentation exhibits the potential to be essential in the diagnosis, prognosis, and treatment plan to effectively manage AD.

Throughout the course of this study, Android Studio was used to develop and test a mobile application that implements the automated segmentation methods of this study (*Figure 10*).
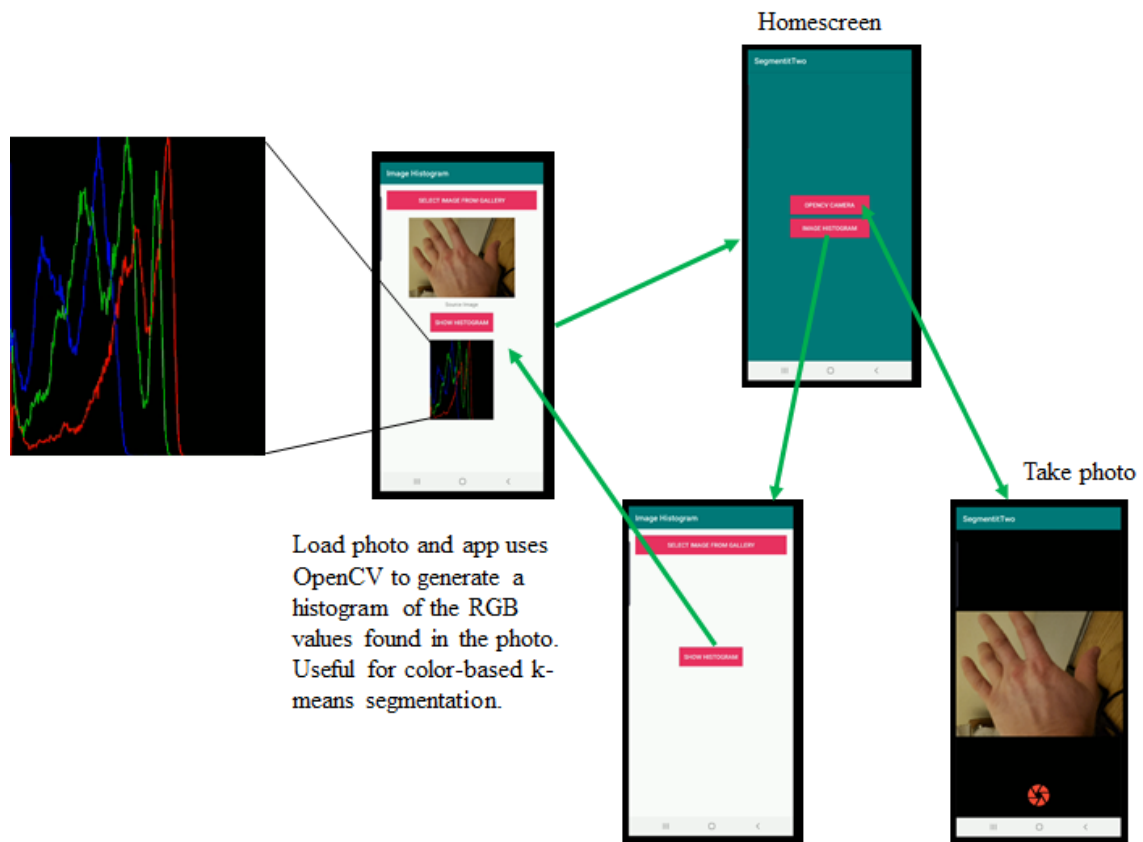
Load photo and app uses OpenCV to generate a histogram of the RGB values found in the photo. Useful for color-based k-means segmentation.

Figure 11. Flowchart of mobile app for k-means based color segmentation of AD

Limitations of this study include the lack of monitoring of the subjects during the 20 days that they were required to photograph their AOIs and a small sample size of 10 subjects. Although, the aspect of images acquired by subjects in their natural setting, at home, is a primary factor in this study, it made it so that the experimenters were unable to determine the level to which subjects followed instructions and the degree to which acquisition bias was a factor between subjects. Future studies may benefit from a

surveillance camera in the subjects home in the location where they will be taking their AOI photographs, so as to document subject behavior and photography procedure. Doing so may enable experimenters to account for and analyze variations in subject self photography of their AOIs.

Although the sample size was small, 10 subjects producing 24 in-lab photos, the three subjects producing 14 at-home photos was not a limitation. As the in-lab photos served as the train dataset for U-Net and at-home photos served as the test dataset, this is a common and acceptable train / test ratio for machine learning models.

The high/low pattern of U-Net results across runs, may be due to the learning rate being set too high. Future directions fine tuning the learning rate and other parameters of U-Net to achieve the most accurate run on the first run. Further development of mobile applications that utilize automated segmentation is a most valuable direction for future studies, as the demand for fast and efficient diagnosis and prognosis grows with improved software and hardware.

REFERENCES

Alam, M. N., Munia, T. T. K., Tavakolian, K., Vasefi, F., MacKinnon, N., & Fazel-
    Rezai, R. (2016). Automatic detection and severity measurement of eczema using
    image processing. In 2016 38th Annual International Conference of the Institute
    of Electrical and Electronics Engineers Engineering in Medicine and Biology
    Society (pp. 1365-1368). *Institute of Electrical and Electronics Engineers*.

Andersson, J., Ahlström, H., & Kullberg, J. (2019). Separation of water and fat signal in
    whole-body gradient echo scans using convolutional neural networks. *Magnetic*
    resonance in medicine, 82(3), 1177-1186.

Bass, R.L. (2019). *Atopic Eczema Treatment*. Retrieved from https://www.eczema-
    ltd.com/atopic.php

Ben-Gashir, M. A., Seed, P. T., & Hay, R. J. (2004). Predictors of atopic dermatitis
    severity over time. *Journal of the American Academy of Dermatology*,*50*(3), 349-
    356.

Ch'ng, Y. K., Nisar, H., Yap, V. V., Yeap, K. H., & Tang, J. J. (2014).
    Segmentation and grading of eczema skin lesions. In 2014 8th
    International Conference on Signal Processing and Communication
    Systems (pp. 1-5). *Institute of Electrical and Electronics Engineers*.

Çiçek, Ö., Abdulkadir, A., Lienkamp, S. S., Brox, T., & Ronneberger, O.
    (2016). 3D U-Net: learning dense volumetric segmentation from sparse
    annotation. In International conference on medical image computing and
    computer-assisted intervention (pp. 424-432). Springer, Cham.

22

Dong, H., Yang, G., Liu, F., Mo, Y., & Guo, Y. (2017). Automatic brain tumor
detection and segmentation using U-Net based fully convolutional
networks. In annual conference on medical image understanding and
analysis (pp. 506-517). Springer, Cham.

Falk, T., Mai, D., Bensch, R., Çiçek, Ö., Abdulkadir, A., Marrakchi, Y., ... &
Dovzhenko, A. (2019). U-Net: deep learning for cell counting, detection,
and morphometry. *Nature Methods*, 16(1), 67.

Fujishima, N., & Hoshino, K. (2012). Fingernail detection in hand images using
difference of nail-color pixels' density between vicinity areas of
fingernails and skin. In The 1st Institute of Electrical and Electronics
Engineers Global Conference on Consumer Electronics 2012 (pp. 233-
237). Institute of Electrical and Electronics Engineers.

Gould, J. (2019). *Label Expansion for AD Treatment*. Retrieved from
https://www.the-dermatologist.com/news/label-expansion-ad-treatment

Hanifin, J. M., Thurston, M., Omoto, M., Cherill, R., Tofte, S. J., Graeber, M.,
& Evaluator Group, T. E. (2001). The eczema area and severity index
(EASI): assessment of reliability in atopic dermatitis. *Experimental
Dermatology*, 10(1), 11-18.

HRPP Policies (2018). Retrieved from http://www.bumc.bu.edu/ohra/hrpp-
policies/hrpp-policies-procedures/#1.1

Kapur, S., Watson, W., & Carr, S. (2018). Atopic dermatitis. *Allergy, Asthma & Clinical Immunology*, 14(2), 52. doi:10.1186/s13223-018-0

Kunz, B., Oranje, A. P., Labreze, L., Stalder, J. F., Ring, J., & Taieb, A. (1997). Clinical validation and guidelines for the SCORAD index: consensus report of the European Task Force on Atopic Dermatitis. *Dermatology*, *195*(1), 10-19.

Lu, J., Kazmierczak, E., Manton, J. H., & Sinclair, R. (2013). Automatic segmentation of scaling in 2-d psoriasis skin images. *Institute of Electrical and Electronics Engineers transactions on medical imaging*, *32*(4), 719-730.

NEA (2019). *What is Eczema?*. Retrieved from https://nationaleczema.org/eczema/

Ning, Y., Shi, C., Wang, L., & Shu, C. (2014, October). Automatic segmentation of psoriasis lesions. In *Optoelectronic Imaging and Multimedia Technology III* (Vol. 9273, p. 927324). International Society for Optics and Photonics.

Nisar, H., Ch'ng, Y. K., Chew, T. Y., Yap, V. V., Yeap, K. H., & Tang, J. J. (2013). A color space study for skin lesion segmentation. In 2013 Institute of Electrical and Electronics Engineers International Conference on Circuits and Systems (pp. 172-176). I*nstitute of Electrical and Electronics Engineers*.

Pal, A., Chaturvedi, A., Garain, U., Chandra, A., Chatterjee, R., & Senapati, S. (2018a). CapsDeMM: Capsule Network for Detection of Munro's Microabscess in Skin Biopsy Images. In International Conference on Medical Image Computing and Computer-Assisted Intervention (pp. 389-397). Springer, Cham.

Pal, A., Garain, U., Chandra, A., Chatterjee, R., & Senapati, S. (2018b). Psoriasis skin

biopsy image segmentation using Deep Convolutional Neural Network.

Computer Methods and Programs in Biomedicine, *159*, 59-69.

Paller, A. S. (2018). Clarification of methodology and further results from the pivotal

phase 3 study of crisaborole for mild-moderate atopic dermatitis. *British*

Journal of Dermatology, 178(3), 663-664. doi:10.1111/bjd.16047

Ramteke, N. S., & Jain, S. V. (2013). ABCD rule based automatic computer-aided skin

cancer detection using MATLAB. *International Journal of Computer*

Applications in Technology,*4*(4), 691-697.

Ronneberger, O., Fischer, P., & Brox, T. (2015). U-net: Convolutional networks for

biomedical image segmentation. In International Conference on Medical image

computing and computer-assisted intervention (pp. 234-241). Springer, Cham.

Salehi, S. S. M., Erdogmus, D., & Gholipour, A. (2017). Auto-context convolutional

neural network (auto-net) for brain extraction in magnetic resonance imaging.

Institute of Electrical and Electronics Engineers transactions on medical

imaging, 36(11), 2319-2330.

Weidinger, S. & Novak, N. (2016). Atopic dermatitis. *The Lancet*, 387(10023), 1109-

1122. doi:10.1016/S0140-6736(15)00149-X

CURRICULUM VITAE